Structural evidence for dimerization-regulated activation of an integral membrane phospholipase

Snijder, H J; Ubarretxena-Belandia, I; Blaauw, M; Kalk, K H; Verheij, H M; Egmond, M R; Dekker, N; Dijkstra, B W

Published in:
Nature

DOI:
10.1038/44890

Publication date:
1999

20. Hendsch, Z. S. & Tidor, B. Do salt bridges stabilize proteins? A continuum electrostatic analysis. *Protein Sci.* **3,** 211–226 (1994).
21. Braden, B. C. & Poljak, R. J. Structural features of the reactions between antibodies and protein antigens. *FASEB J.* **9,** 9–16 (1995).
22. Covell, D. G. & Wallqvist, A. Analysis of protein–protein interactions and the effects of amino acid mutations on their energetics: the importance of water molecules in the binding epitope. *J. Mol. Biol.* **269,** 281–297 (1997).
23. Kuga, T. *et al.* Japanese Patent Publication (Kokoku) 8317 Feb. 2 (1994).
24. Yamasaki, M., Konishi, N., Yamaguchi, K., Itoh, S. & Yokoo, Y. Purification and characterization of recombinant human granulocyte colony-stimulating factor (rhG-CSF) derivatives: KW-2228 and other derivatives. *Biosci. Biotechnol. Biochem.* **62,** 1528–1534 (1998).
25. Livnah, O. *et al.* An antagonist peptide–EPO receptor complex suggests that receptor dimerization is not sufficient for activation. *Nature Struct. Biol.* **5,** 993–1004 (1998).
26. Livnah, O. *et al.* Crystallographic evidence for preformed dimers of erythropoietin receptor before ligand activation. *Science* **283,** 987–990 (1999).
27. Remy, I., Wilson, I. A. & Michnick, S. W. Erythropoietin receptor activation by a ligand-induced conformation change. *Science* **283,** 990–993 (1999).
28. Otwinowski, Z. & Minor, W. Processing of X-ray diffraction data collected in oscillation mode. *Methods Enzymol.* **276,** 307–326 (1997).
29. Collaborative Computational Project, Number 4. The CCP4 Suite: Programs for crystallography. *Acta Crystallogr. D* **50,** 760–763 (1994).
30. Brünger, A. T. X-PLOR, Version 3.1, *A System for X-ray Crystallography and NMR* (Yale Univ. Press, New Haven, 1992).

Acknowledgements

We thank N. Kamiya and M. Kawamoto for their help in the use of the data collection facilities at SPring-8, Hyogo, Japan, and N. Sakabe and N. Watanabe for use of the facilities at Photon Factory, Tsukuba, Japan. We thank S. Nagata for providing the GCSFR cDNA, E. Yanagihara and N. Okitsu for assistance in sample preparation, and Y. Kato, D. Kohda, H. Toh, K. Yamasaki and S. Tsutakawa for useful discussions. This study was partly supported by a grant from TARA (Tsukuba Advanced Research Alliance), University of Tsukuba, Japan.

Correspondence and requests for materials should be addressed to K.M. (e-mail: morikawa@beri.co.jp). Coordinates have been deposited in the Brookhaven Protein Data Bank, accession codes 1cd9 for the $I4_122$ and 1pgr for the $P4_32_12$ form.

Structural evidence for dimerization-regulated activation of an integral membrane phospholipase

H. J. Snijder*, I. Ubarretxena-Belandia†‡, M. Blaauw*‡, K. H. Kalk*, H. M. Verheij†§, M. R. Egmond†, N. Dekker† & B. W. Dijkstra*

** Laboratory of Biophysical Chemistry, BIOSON Research Institute, University of Groningen, Nijenborgh 4, 9747 AG Groningen, The Netherlands*
† Department of Enzymology and Protein Engineering, Centre for Biomembranes and Lipid Enzymology, Institute of Biomembranes, Utrecht University, Padualaan 8, 3584 CH Utrecht, The Netherlands

Dimerization is a biological regulatory mechanism employed by both soluble and membrane proteins[1]. However, there are few structural data on the factors that govern dimerization of membrane proteins. Outer membrane phospholipase A (OMPLA) is an integral membrane enzyme which participates in secretion of colicins in *Escherichia coli*. In *Campilobacter*[2] and *Helicobacter pylori* strains[3], OMPLA is implied in virulence. Its activity is regulated by reversible dimerization[4,5]. Here we report X-ray structures of monomeric and dimeric OMPLA from *E. coli*. Dimer interactions occur almost exclusively in the apolar membrane-embedded parts, with two hydrogen bonds within the hydrophobic membrane area being key interactions. Dimerization results in functional oxyanion holes and substrate-binding pockets, which are absent in monomeric OMPLA. These results provide a detailed view of activation by dimerization of a membrane protein.

The structure of monomeric OMPLA consists of a 12-stranded antiparallel β-barrel with a convex and a flat side (Fig. 1a). The 12 amphipathic β-strands traverse the membrane, forming a hydrophobic outer surface flanked by rings of aromatic residues at the polar–apolar boundaries of the membrane bilayer. Loops (L1–L6) join consecutive strands at the extracellular side, and turns (T1–T5) connect the strands at the periplasmic side of the membrane (as inferred from epitope insertion studies[6]). The interior of the β-barrel is polar and contains an intricate hydrogen-bonding network providing a rigid structure. The two termini and the L1, L4 and L6 loops cover the barrel's interior and obstruct pore function, as corroborated by the absence of pore activity in black-lipid films (N.D., unpublished results). The 12-β-stranded architecture of OMPLA resembles the folds of other β-barrel outer membrane proteins[7–11] that have 8–22 β-strands. This shows the functionality of this fold not only for transport and structural proteins but also for membrane enzymes.

The active site contains Ser 144 and His 142, as established from chemical modification[12] and site-directed mutagenesis experiments[13,14], and is located on the exterior of the β-barrel, positioned just outside the outer leaflet ring of aromatic residues. Besides the serine and histidine, the active site contains an asparagine residue (Asn 156). Its side chain is at hydrogen-bonding distance from the Nδ1 atom of His 142, fixing the orientation of the His 142 side chain. This constellation of active-site residues resembles that of classical serine hydrolases[15], but with a neutral asparagine instead of an aspartate residue. Mutation studies have confirmed the importance of Asp 156 for catalysis (R. L. Kingma *et al.*, manuscript in preparation).

Reversible dimerization regulates the activity of OMPLA, with the dimer being the active species[4,5]. Covalent inhibition with hexadecanesulphonylfluoride allowed the crystallization of the dimeric enzyme. The structural rearrangements upon dimerization are surprisingly few and small (r.m.s. difference between monomer and dimer is 0.4 Å for 257 Cα atoms). The monomers (labelled A and B) associate with the flat sides of their β-barrels to form a homodimer (Fig. 2a), such that both active sites are located at the outer leaflet side of the membrane. Roughly 1,100 $Å^2$ of the accessible surface is buried, which corresponds to 10% of the total surface. All interactions between the monomers occur in the hydrophobic membrane-embedded area (Fig. 2b), except for three main-chain hydrogen bonds formed at the polar–apolar membrane boundary (Phe 109^A–Gly 146^B, Gly 146^A–Phe 109^B and Leu 32^A–Leu 32^B). The hydrophobic side chains of Leu $32^{A/B}$, Leu $71^{A/B}$, Leu $73^{A/B}$ and Leu $265^{A/B}$ exhibit a knob-and-hole interaction. Residues Tyr $114^{A/B}$–Phe $109^{B/A}$ have aromatic stacking interactions with contact distances as close as 3.5 Å. The tyrosine hydroxyl groups point towards a cavity with a hydrophilic character extending deep into the hydrophobic membrane-embedded area. The cavity is lined with the side chains of Tyr $92^{A/B}$, Gln $94^{A/B}$, Ser $96^{A/B}$ and Thr $112^{A/B}$. In monomeric OMPLA, a stabilizing hydrogen-bond network between Tyr 92, Gln 94 and Ser 96 allows these residues to partition in the hydrophobic membrane environment. In the dimer, however, the side chain of Gln 94 is additionally hydrogen bonded to Gln 94 of the other monomer (Fig. 1b). Gln 94 is strictly conserved in all OMPLA sequences, emphasizing the importance of this residue for functional dimerization. Thus, specific dimer interactions are obtained from a combination of surface complementarity of knob-and-hole patterns and hydrogen-bonding interactions between polar residues in the hydrophobic membrane environment. Similar polar patches have been observed in the apolar membrane-embedded regions of other membrane proteins[8,10,11], but here we show for the first time, to our knowledge, their participation in protein–protein interactions.

Dimerization results in productive active sites, with two substrate-binding pockets created at the interface between the two

‡ Present addresses: Molecular Biophysics and Biochemistry, Yale University, 429 Bass Center, 266 Whitney Avenue, New Haven, Connecticut 06520, USA (I.U.B.); Department of Biochemistry, University of Groningen, Nijenborgh 4, 9747 AG Groningen, The Netherlands (M.B.).
§ H.M.V. died in an accident on 1 August 1998.

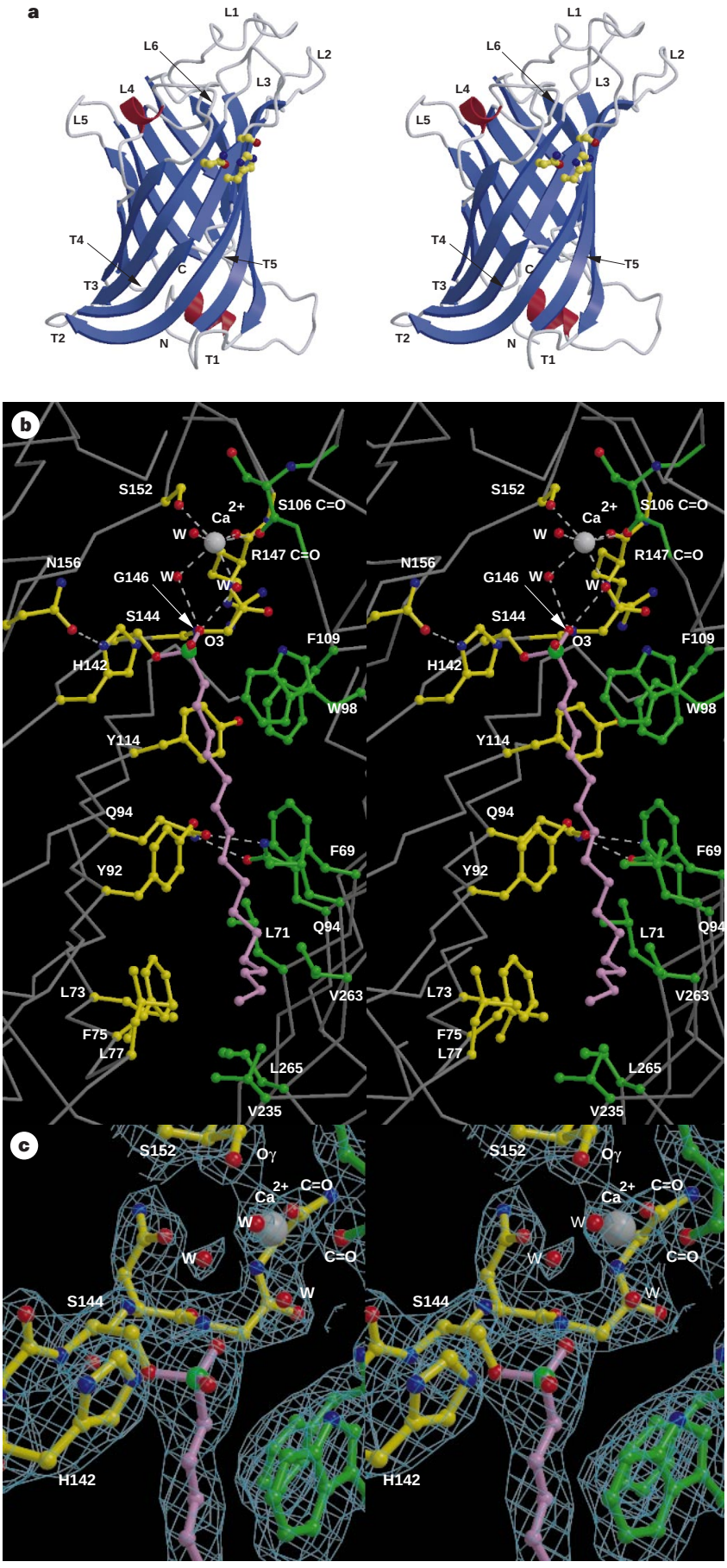

Figure 1 Structure of outer membrane phospholipase A. **a**, Stereo drawing of the secondary structure of a monomer. The α-helices, β-strands and turns are depicted in red, blue and grey, respectively. Loops and turns are numbered from the N to C terminus and defined as L1, residues 46–64; L2, 99–108; L3, 145–153; L4, 179–196; L5, 215–221; L6, 246–254; T1, 80–85, T2, 129–130; T3, 167–168; T4, 204–205; and T5, 231–235. The active-site residues (ball-and-stick representation) are located at the exterior of the β-barrel, facing the outer leaflet side of the membrane. **b**, Stereo diagram of the active site and binding pocket of OMPLA. The inhibitor and residues from monomer A and B are coloured in purple, yellow and green, respectively. Dashed lines indicate hydrogen bonds in the active site; in the calcium-binding site and between the two glutamines Gln $94^{A/B}$ involved in dimer interaction. The calcium ion is shown; unexpectedly, none of its ligands is charged. **c**, Stereo diagram of the electron density in the active site of dimeric OMPLA with $2F_0F_c$ OMIT electron density contoured at 1σ level.

monomers. Both pockets accommodate all 16 aliphatic carbon atoms of the inhibitors (Figs 1b and 2b). Aromatic residues Tyr 114^{A}, Phe 109^{B} and Trp 98^{B} contact the upper three carbon atoms of the inhibitor. The side chains of Tyr 92^{A}, Phe 69^{B} and Leu 40^{B} line the substrate-binding site for carbon atoms six to eight of the inhibitor. After a bend at residues Leu 71^{B} and Leu 265^{B} (Figs 1b and 2b), the remainder of the binding pocket is lined with residues Phe 75^{A}, Leu 77^{A}, Val 235^{B} and Val 236^{B}, illustrating the exclusively hydrophobic character of the binding pocket. Both monomers contribute to binding the inhibitor. In particular, contacts for carbon atoms 10–16 are provided by the neighbouring molecule. Binding of the inhibitors accounts for 27% of the dimerization surface, which rationalizes the observed increase in dimer stability of the inhibited enzyme[4].

The catalytic sites are located at the top end of each substrate-binding pocket, where a cup-like structure is formed at the interface of the monomers (Fig. 1b). The base of the active site consists of Tyr 114^{A}, Trp 98^{B} and Phe 109^{B}. The walls are formed by the active site His 142^{A}, the amino-terminal residues of β-strand 6^{A} and loops L2^{B}, L3^{A} and L4^{A}. The sulphonyl moiety of the inhibitor is located in the centre of this active-site cup, where it is covalently bound to the Oγ of the nucleophilic serine (Fig. 1c). It mimics the transient tetrahedral intermediate of the deacylation step in the serine hydrolase catalytic mechanism. The O3 sulphonyl oxygen atom is at hydrogen-bonding distance from the main-chain nitrogen atom of Gly 146^{A} and two^{A} (or one^{B}) water molecules. These water molecules are bound, in turn, to a calcium ion present in the active site. Calcium is an essential cofactor for activity[16] and dimerization[4]. Its binding site is located at the dimer interface and the ion has ligands from both monomers (main-chain carbonyl oxygen atoms from Arg 147^{A} and Ser 106^{B}, the Oγ atom of Ser 152^{A} and three water molecules; Figs 1c and 3). Ser 152 is essential for catalysis[14]. The structure indicates that the catalytic importance of this residue may be related to its calcium-ligating capacity. Despite biochemical evidence for a second calcium site[16], we find only one bound calcium ion per monomer, presumably caused by the enzyme's low calcium affinity in the presence of uncharged detergents[16].

A phospholipid substrate may bind to OMPLA in a similar fashion to the inhibitor, with one acyl chain occupying the position of the inhibitor's aliphatic chain. The second acyl chain may be located in the membrane compartment without the need for a particular binding site. The phosphate group of the substrate probably extends towards the solvent and could bind to the calcium ion; however, catalysis requires neither the second acyl chain nor the phosphate group[17], explaining the absence of obvious binding sites for them. Hydrolysis of the substrate could proceed through a mechanism analogous to that of serine hydrolases, with Ser 144 performing a nucleophilic attack on the carbonyl carbon of the ester. A negatively charged intermediate will then be formed which is stabilized by a tetrahedral arrangement of hydrogen bonds (the amide of Gly 146 and two water molecules) and by the remote influence of the calcium ion (at 4.3 Å). The transient intermediate will then collapse to give the enzyme-acyl intermediate. The lyso-phospholipid product can now leave the active site by lateral diffusion into the membrane. Likewise, deacylation occurs with a water molecule acting as nucleophile. The fatty-acid product may leave the active site either by lateral diffusion into the membrane through the opening between His 142^{A} and Trp 98^{B} (Fig. 1b) or after dissociation of the dimer. Calcium may have a triple role in catalysis. It may increase the nucleophilicity of the serine, it could polarize the ester carbonyl bond, thereby facilitating nucleophilic attack, and it is involved in oxyanion stabilization. A comparable active site and well-developed oxyanion stabilization have been observed in *Streptomyces scabies* esterase[18], which relies on a His-Ser dyad with an carbonyl oxygen atom stabilizing the histidine, and three tetrahedrally arranged hydrogen bonds coordinating the oxyanion (Fig. 3).

Both calcium[4] and substrate[19] govern dimerization. The main factor that controls dimerization *in vivo* is probably the substrate. Normally, phospholipids are only present in the inner leaflet of the outer membrane, and OMPLA is in the inactive monomeric form[5]. As activation of OMPLA concurs with the perturbation of the bacterial membrane[4], we propose that the relief of lipid asymmetry and the presentation of substrate to the outer leaflet induces activation by promoting dimerization and calcium binding. The OMPLA dimer then hydrolyses the substrate into lyso-phospholipids and fatty acids. These compounds will further destabilize the membrane bilayer, and may thus facilitate the release of colicins or virulence factors.

In conclusion, our work shows that, even in the membrane-embedded parts of integral membrane proteins, polar interactions can contribute to specific intermolecular contacts. These can be seen as the membrane equivalent of burying hydrophobic side chains in the binding interface of soluble proteins. Our findings could aid in the understanding of a wide variety of activation and regulation

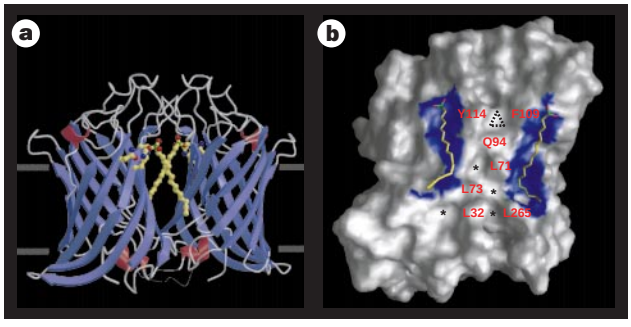

Figure 2 Dimer covalently inhibited with hexadecanesulphonylfluoride. **a**, Diagram of dimer with active-site residues and inhibitor shown in ball-and-stick representation. Residues 25–31 which lack interpretable density are indicated by thin dashed lines. The polar–apolar membrane boundaries are roughly indicated in grey. **b**, Surface representation of the dimerization interface of one monomer. The surface area within 1.5 Å of the van der Waals surface of the inhibitors is depicted in blue. The inhibitor on the left is covalently bound to Ser 144 of the monomer shown; the inhibitor on the right belongs to the monomer that is omitted in this diagram. Residues that are involved in the dimer interaction in the membrane-embedded part are indicated. Asterisks indicate the holes from the knob-and-hole pattern. The dashed triangle indicates the hydrophilic cavity (see text).

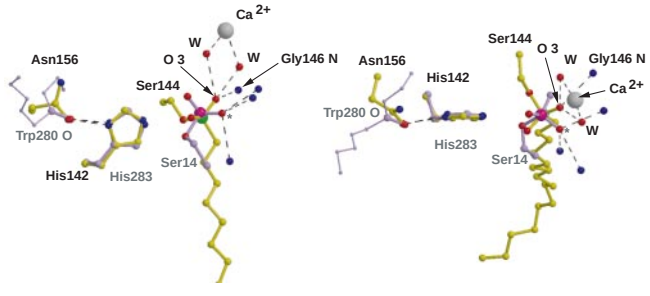

Figure 3 Comparison of the catalytic machinery of OMPLA and *Streptomyces scabies* esterase. Two orthogonal views show superimposition of the imidazole rings and carboxamide (Asn 156) and carbonyl (Trp 283) oxygen atoms; however, the orientation of the serine residues, inhibitors and oxyanion holes is mirrored with respect to each other. OMPLA is shown in yellow with black labels; *S. Scabies* esterase is shown in purple with grey labels. Oxyanion-hole ligands are shown but labelled only for OMPLA; the oxygen O3 atom proposed to correspond to the oxyanion is indicated. The corresponding oxygen in the *S. scabies* esterase is indicated with an asterisk.

Table 1 Data collection and phasing statistics

	Monomer			Ir-3 λ1	Ir-3 λ2	Ir-3 λ3	Se-Met λ1	Se-Met λ2	Se-Met λ3	Dimer
	Set 1	Set 2	Set 3							
Resolution (Å)	36.6–2.5	18.1–2.2	3.5–2.2	20.0–3.2	20.0–3.1	20.0–30	19.0–2.8	19.0–2.8	19.0–2.8	20.3–2.1
Wavelength (Å)	0.9164	0.9901	0.9901	1.10394	1.10444	0.827	0.97891	0.97969	0.90	0.99385
No. of unique, reflections	10973	13581	7532	6585	7244	7598	9365	9013	8161	28336
Redundancy	8.4	5.9	7.0	7.3	7.1	5.9	3.4	3.7	2.9	2.69
Completeness (%)	81.7 (42.6)	69.4 (4.1)	51.9 (5.2)	97.1 (92.1)	93.2 (81.2)	93.2 (77.8)	95.5 (95.8)	96.8 (93.5)	87.5 (91.8)	74.1 (66.3)
R_{sym}* (%)	4.1 (33.6)	4.9 (15.9)	9.0 (13.4)	9.8 (26.3)	7.1 (26.1)	6.1 (29.9)	5.4 (28.3)	5.9 (28.5)	5.7 (31.8)	7.7 (26.5)
⟨I⟩/⟨s(I)⟩	17.2 (2.9)	18.1 (2.8)	10.9 (3.7)	15.7 (2.6)	22.0 (4.2)	25.0 (3.7)	14.7 (3.3)	15.6 (3.5)	11.5 (2.4)	10.9 (2.3)
R_{iso}† (%)				18.2	17.1	18.6	14.8	14.8	16.2	
No. of sites				2	2	2	5	5	5	
Phasing power‡ acentric/centric				1.95/1.12	1.96/1.50	2.13/1.60	1.23/0.77	1.15/0.90	1.51/1.00	
R_{cullis}§ iso				0.67/0.74	0.66/0.75	0.64/0.72	0.81/0.77	0.83/0.72	0.77/0.81	
R_{cullis}§ ano				0.79	0.80	0.78	0.78	0.93	0.87	
Beam line	X11	D2AM	D2AM	X31	X31	X31	X31	X31	X31	ID2B

Refinement statistics

	Monomer	Dimer
Resolution range (Å)	36.6–2.2	20.3–2.1
Total no. of nonhydrogen atoms	2231	4220
No. of water molecules	28	69
R-factor (%)	22.1	22.6
Free *R*-factor (%)	27.0	28.3
Average *B*-factor (Å^2)	56.0	34.5
R.m.s.d. bond lengths (Å)	0.005	0.007
R.m.s.d. bond angles	1.3°	1.2°

*$R_{sym} = \Sigma_{hkl}\Sigma_{sym}|F - \langle F\rangle|/\Sigma_{hkl}F$.
†$R_{iso} = \Sigma_{hkl}|F_{der} - F_{nat}|/\Sigma_{hkl}F_{nat}$.
‡Phasing power $= \Sigma_{hkl}|F_h|/\Sigma_{hkl}|E| = \Sigma_{hkl}|F_h|/\Sigma_{hkl}||F_{ph_{obs}}| - |F_{ph_{calc}}||$ = ⟨F_h/loc⟩.
§$R_{cullis} = \Sigma_{hkl}||F_{ph_{obs}}| - |F_{ph_{calc}}||/\Sigma_{hkl}|F_{ph} - F_p|$isomorphous = ⟨loc⟩/⟨iso. diff⟩.
§$R_{cullis} = \Sigma_{hkl}||F^+ - F^-| - (2 \times |F_h''\text{calc}|)|/\Sigma_{hkl}||F^+ - F^-|$ anomalous = ⟨loc⟩/⟨ano. diff⟩.

processes, such as signal transduction, phospholipid metabolism and bacterial pathogenicity. □

Methods

Crystallization

Crystals of monomeric OMPLA (relative molecular mass 31K; 269 amino acids) were obtained by mixing protein solution (8 mg ml^{-1} OMPLA, 10 mM succinate buffer pH 6.5, 1.5% 1-O-*n*-octyl-β-D-glucopyranoside (β-OG), 1 mM NaN_3) in a 3:2 ratio with a reservoir solution containing 25–29% (v/v) 2-methyl-2,4-pentanediol, 1 mM $CaCl_2$ and 0.1 M bis-Tris pH 5.9–6.0 (ref. 20). The space group of the crystals was $P3_121$ with cell dimensions $a = b = 78.55$, $c = 101.52$ Å. The protein labelled with selenomethionine crystallized under similar conditions to the wild-type protein.

Crystals of dimeric OMPLA were obtained by covalent modification of the active-site serine by the inhibitor hexadecanesulphonylfluoride[12] before crystallization. Crystals were grown from 10 mg ml^{-1} inhibited protein solution containing 1.95% (w/v) β-OG, 10 mM KCl, 2 mM Tris pH 6.6 equilibrated against 12–17% (v/v) PEG400. Crystals of the inhibitor–enzyme complex were soaked for 20 min in a solution containing 0.5% (w/w) β-OG, 70% (w/w) phytohistol (Roth) and 15 mM $CaCl_2$ before data collection. These crystals were flash frozen using phytohistol as a cryoprotectant. The crystals belong to space group $P2_12_12_1$ with cell dimensions $a = 81.54$ Å, $b = 84.97$ Å and $c = 95.80$ Å, and have two molecules in the asymmetric unit.

Data collection and processing

Native data of monomeric OMPLA were collected on cryopreserved crystals at EMBL beam line X11, DESY, Hamburg (data set 1) and at the D2AM beam line at the ESRF, Grenoble (data sets 2 and 3). Data were processed using DENZO/SCALEPACK[21] for data set 1, and XDS[22] for data sets 2 and 3. The three data sets were merged using KBRANI (BIOMOL software package); data collected on the D2AM beam line were merged first (R_{merge} 7.7%) and subsequently merged with data set 1 (R_{merge} 10.5%). The crystals diffracted anisotropically, resulting in an effective resolution of the merged data of about 2.4 Å. An iridium derivative was prepared by soaking a native crystal in stabilizing mother liquor at pH 6.5 with 10 mM Na_3IrCl_6 for one day, which gave two unique sites. Three-wavelength anomalous dispersion experiments were collected on the iridium and selenomethione derivatives at EMBL beam line X31, DESY, Hamburg. These data were processed with DENZO/SCALEPACK[21] and scaled with KBRANI. Data on a dimer crystal was collected to 2.1 Å at the ID2B beam line at the ESRF, Grenoble, and processed with DENZO/SCALEPACK[21]. Crystallographic data are summarized in Table 1.

Structure determination

Isomorphous differences between derivatives and native data were included in phasing, in addition to the MAD phase information. Phases calculated with MLPHARE[23] were improved by solvent flipping and histogram matching using DM[23]. The resulting electron-density map allowed placement of residues 13–269. The model was refined using the slow-cooling protocol and conjugate gradient positional refinement in X-PLOR[24] cycled with manual rebuilding using O[25]. Bulk solvent correction, overall anisotropic *B*-factor scaling and a resolution-dependent weighting were applied, and temperature factors were refined individually. The model further comprises 28 water molecules and 5 partly occupied β-OG molecules. The final *R* and R_{free} of the model are 22.0% and 27.1%, respectively. Remaining difference density around the protein molecule was interpreted as disordered detergent. 84.8% of the main-chain phi–psi torsion angles is in the most favoured regions, whereas none is in disallowed regions of the Ramachandran plot.

Phases for the dimer were obtained by molecular replacement (AMoRE[23]) using the monomer as a search model. The dimer was refined using a slow-cooling protocol and conjugate gradient positional refinement in X-PLOR[24] cycled with minor rebuilding using O[25]. Bulk solvent correction, overall anisotropic *B*-factor scaling, and a resolution-dependent weighting were applied. Initially, tight non-crystallographic symmetry (NCS) restraints were applied to the entire molecules, but later these restraints were gradually relieved. Water molecules were included in the model. Two water molecules with exceptionally low *B*-factors and substantial difference density were interpreted as calcium ions. Restrained individual temperature factor refinement resulted in a final *R* of 22.6% and R_{free} of 28.3%. Molscript[26] was used to produce Figs 1a, b, 2a and 3; Raster3D[27] was used for all figures except Fig. 2b; GRASP[28] was used for Fig. 2b; and the program Bobscript[29] was used for Fig. 1c.

Received 7 May; accepted 6 August 1999.

1. Klemm, J. D., Schreiber, S. L. & Crabtree, G. R. Dimerization as a regulatory mechanism in signal transduction. *Annu. Rev. Immunol.* **16,** 569–592 (1998).
2. Grant, K. A., Ubarretxena-Belandia, I., Dekker, N., Richardson, P. T. & Park, S. F. Molecular characterization of *pldA*, the structural gene for a phospholipase A from *Campylobacter coli*, and its contribution to cell-associated hemolysis. *Infect. Immun.* **65,** 1172–1180 (1997).
3. Bukholm, G. *et al.* Colony variation of *Helicobacter pylori*: pathogenic potential is correlated to cell wall lipid composition. *Scan. J. Gastroenterol.* **32,** 445–454 (1997).
4. Dekker, N., Tommassen, J., Lustig, A., Rosenbusch, J. P. & Verheij, H. M. Dimerization regulates the enzymatic activity of *Escherichia coli* outer membrane phospholipase A. *J. Biol. Chem.* **272,** 3179–3184 (1997).
5. Dekker, N., Tommassen, J. & Verheij, H. M. Bacteriocin release protein triggers dimerization of outer membrane phospholipase A *in vivo*. *J. Bacteriol.* **181,** 3281–3283 (1999).
6. Merck, K. B., de Cock, H., Verheij, H. M. & Tommassen, J. Topology of the outer membrane phospholipase A of *Salmonella typhimurium*. *J. Bacteriol.* **179,** 3443–3450 (1997).
7. Weiss, M. S. *et al.* Molecular architecture and electrostatic properties of a bacterial porin. *Science* **254,** 1627–1630 (1991).
8. Schirmer, T., Keller, T. A., Wang, Y.-F. & Rosenbusch, J. P. Structural basis for sugar translocation through maltoporin channels at 3.1 Å resolution. *Science* **267,** 512–514 (1995).
9. Pautsch, A. & Schulz, G. E. Structure of the outer membrane protein A transmembrane domain. *Nature Struct. Biol.* **5,** 1013–1017 (1998).
10. Locher, K. P. *et al.* Transmembrane signaling across the ligand-gated FhuA receptor: Crystal structures of free and ferrichrome-bound states reveal allosteric changes. *Cell* **95,** 771–778 (1998).
11. Buchanan, S. K. *et al.* Crystal structure of the outer membrane active transporter FepA from *Escherichia coli*. *Nature Struct. Biol.* **6,** 56–63 (1999).
12. Horrevoets, A. J., Verheij, H. M. & de Haas, G. H. Inactivation of *Escherichia coli* outer-membrane phospholipase A by the affinity label hexadecanesulfonyl fluoride. Evidence for an active-site serine. *Eur. J. Biochem.* **198,** 247–253 (1991).
13. Brok, R. G. P. M., Dekker, N., Gerrits, N., Verheij, H. M. & Tommassen, J. A conserved histidine

residue of *Escherichia coli* outer-membrane phospholipase A is important for activity. *Eur. J. Biochem.* **234,** 934–938 (1995).
14. Brok, R. G. P. M., Ubarretxena-Belandia, I., Dekker, N., Tommassen, J. & Verheij, H. M. *Escherichia coli* outer membrane phospholipase A: Role of two serines in enzymatic activity. *Biochemistry* **35,** 7787–7793 (1996).
15. Dodson, G. & Wlodawer, A. Catalytic triads and their relatives. *Trends Biochem. Sci.* **23,** 347–352 (1998).
16. Ubarretxena-Belandia, I., Boots, J. W. P., Verheij, H. M. & Dekker, N. Role of the cofactor calcium in the activation of outer membrane phosphilipase A. *Biochemistry* **37,** 16011–16018 (1998).
17. Horrevoets, A. J. G., Hackeng, T. M., Verheij, H. M., Dijkman, R. & De Haas, G. H. Kinetic characterization of *Escherichia coli* outer membrane phospholipase A using mixed detergent-lipid micelles. *Biochemistry* **28,** 1139–1147 (1989).
18. Wei, Y. *et al.* A novel variant of the catalytic triad in the *Streptomyces scabies* esterase. *Nature Struct. Biol.* **2,** 218–223 (1995).
19. Ubarretxena-Belandia, I. *et al.* Outer membrane phospholipase A is dimeric in phospholipid bilayers: A cross-linking and fluorescence resonance energy transfer study. *Biochemistry* **38,** 7398–7405 (1999).
20. Blaauw, M., Dekker, N., Verheij, H. M., Kalk, K. H. & Dijkstra, B. W. Crystallization and preliminary X-ray analysis of outer membrane phospholipase A from *Escherichia coli*. *FEBS Lett.* **373,** 10–12 (1995).
21. Otwinowski, Z. & Minor, W. Processing of X-ray diffraction data collected in oscillation mode. *Methods Enzymol.* **276,** 307–326 (1997).
22. Kabsch, W. Automatic processing of rotation diffraction data from crystals of initially unknown symmetry and cell constants. *J. Appl. Crystallogr.* **26,** 795–800 (1993).
23. Collaborative Computational Project Number 4. The CCP4 suite: programs for protein crystallography. *Acta Crystallogr. D* **50,** 760–763 (1994).
24. Brünger, A. T. Free *R* value: a novel statistical quantity for assessing the accuracy of structures. *Nature* **355,** 472–475 (1992).
25. Jones, T. A., Zou, J.-Y., Cowan, S. W. & Kjeldgaard, M. Improved methods for building protein models in electron density maps and the location of errors in these models. *Acta Crystallogr. A* **47,** 110–119 (1991).
26. Kraulis, P. J. MOLSCRIPT: a program to produce both detailed and schematic plots of protein structures. *J. Appl. Crystallogr.* **24,** 946–950 (1991).
27. Merritt, E. A. & Bacon, J. A. Raster3D: photorealistic molecular graphics. *Methods Enzymol.* **277,** 505–524 (1997).
28. Nicholls, A., Sharp, K. A. & Honig, B. Protein folding and association: insights from the interfacial and thermodynamic properties of hydrocarbons. *Proteins Struct. Funct. Genet.* **11,** 281–296 (1991).
29. Esnouf, R. M. An extensively modified version of Molscript that includes greatly enhanced coloring capabilities. *J. Mol. Graphics* **15,** 132–134 (1997).

Acknowledgements

We thank the staff at the EMBL-outstation at DESY in Hamburg, and at the D2AM and the ID2B beam lines at ESRF Grenoble, for assistance with data collection. We thank R. L. Kingma for her enthusiastic collaboration and discussions. We thank the ESRF for supporting the work at the ESRF. These investigations were supported by the Netherlands Foundation for Chemical Research (CW) with financial aid from the Netherlands Organization for Scientific Research (NWO). We thank the EU for supporting the work at EMBL Hamburg through the HCMP Access to Large Installations Project.

Correspondence and requests for materials should be addressed to B.W.D. Coordinates have been deposited in the Protein Data Bank under accession numbers 1QD5 and 1QD6.

The reaction cycle of isopenicillin *N* synthase observed by X-ray diffraction

Nicolai I. Burzlaff*†, Peter J. Rutledge*†, Ian J. Clifton*, Charles M. H. Hensgens*, Michael Pickford‡, Robert M. Adlington*, Peter L. Roach* & Jack E. Baldwin*

* *The Dyson Perrins Laboratory and the Oxford Centre for Molecular Sciences, University of Oxford, South Parks Road, Oxford, OX1 3QY, UK*
‡ *The Laboratory of Molecular Biophysics, University of Oxford, South Parks Road, Oxford, OX1 3QY, UK*
† *These authors contributed equally to this work*

Isopenicillin *N* synthase (IPNS), a non-haem iron-dependent oxidase, catalyses the biosynthesis of isopenicillin *N* (IPN), the precursor of all penicillins and cephalosporins[1]. The key steps in this reaction are the two iron-dioxygen-mediated ring closures of the tripeptide δ-(L-α-aminoadipoyl)-L-cysteinyl-D-valine (ACV). It has been proposed that the four-membered β-lactam ring forms initially, associated with a highly oxidized iron(IV)-oxo (ferryl) moiety, which subsequently mediates closure of the five-membered thiazolidine ring[2]. Here we describe observation of the IPNS reaction in crystals by X-ray crystallography. IPNS·Fe^{2+}·substrate crystals were grown anaerobically[3,4], exposed to high pressures of oxygen to promote reaction and frozen, and their structures were elucidated by X-ray diffraction. Using the natural substrate ACV, this resulted in the IPNS·Fe^{2+}·IPN product complex. With the substrate analogue, δ-(L-α-aminoadipoyl)-L-cysteinyl-L-*S*-methyl-cysteine (ACmC) in the crystal, the reaction cycle was interrupted at the monocyclic stage. These mono- and bicyclic structures support our hypothesis of a two-stage reaction sequence leading to penicillin. Furthermore, the formation of a monocyclic sulphoxide product from ACmC is most simply explained by the interception of a high-valency iron-oxo species.

A challenge in protein crystallography is the possibility of directly observing the structural changes occurring in enzymes during the catalytic cycle. One approach has been the use of Laue crystallography, which has permitted the observation of relatively small changes in structure, such as the photodissociation of a small ligand[5]. The IPNS-catalysed oxidative synthesis of IPN involves significant movements of atoms, through the formation of the two fused heterocyclic rings of penicillin from the linear precursor ACV. Our approach involved the direct oxygenation of anaerobically grown crystals of IPNS complexed with Fe^{2+} and substrates, then structural investigation by X-ray crystallography.

In solution, IPNS shows relatively slow kinetic parameters ($k_{cat} = 4.6\ s^{-1}$, $K_m = 0.56$ mM for ACV, where k_{cat} is the maximum catalytic rate when substrate is saturating, and K_m is the concentration of substrate at which the reaction rate is half its maximum value[6], and initial experiments with crystals exposed to atmospheric pressures of oxygen (air) proved unsuccessful. Therefore, a 'bomb' suitable for exposing crystals to oxygen at pressures up to 60 bar was built[7,8], and used to expose crystals of IPNS·Fe^{2+}·ACV to 40-bar oxygen for different time periods. After an exposure time of 20 min, a transient pale yellow colour (λ_{max} 410 nm) was observed uniformly across the crystals; the colour faded with prolonged exposure and was no longer discernible after 320 min. The origin of this chromophore is at present uncertain, but a similar absorption (λ_{max} 430 nm) has been attributed to a ferryl species in methane monooxygenase[9], although that enzyme has a di-iron centre.

A single crystal of IPNS·Fe^{2+}·ACV exposed to the same oxygen pressure for 320 min allowed determination of the structure of IPNS·Fe^{2+}·IPN to 1.35 Å resolution (Fig. 1a, b). The structure is primarily that of an IPNS·Fe^{2+}·IPN product complex, but residual electron density at the carbonyl and sulphide regions of the ACV cysteine unit make it apparent that the crystal still contains 30% of unreacted IPNS·Fe^{2+}·ACV (Fig. 1b). Attempts to obtain complete turnover by extended pressurization under oxygen (for up to 640 min) were unsuccessful. Crystals exposed for these longer times showed low occupancy in the substrate binding region, consistent with slow release of the product from the active site into the surrounding solvent.

The most significant differences between the IPNS·Fe^{2+}·IPN structure and the IPNS·Fe^{2+}·ACV complex are in the positions of the β-lactam carbonyl group and the cysteinyl sulphur atom. The carbonyl group has moved 60° around the axis of the cysteinyl C_1–C_2 bond, towards Phe 211. The absence of well-ordered hydrogen bonds to this carbonyl group in the substrate complex appears necessary to facilitate this movement. During the reaction, the sulphur migrates around the iron towards the valine β-carbon and out of the site *trans* to His 270, forming the pentacoordinate product complex. A cavity apparent in the IPNS·Fe^{2+}·ACV complex accommodates the sulphur in the product structure. The valine isopropyl group has rotated about the C_α–C_β bond to facilitate formation of the carbon–sulphur bond, and this rotation reverses